Prototyping of a real size air-conditioning system using a tetra-n-butylammonium bromide semiclathrate hydrate slurry as secondary two-phase refrigerant - Experimental investigations and modelling // Prototypage d'un système de conditionnement d'air de taille réelle utilisant un coulis d'hydrate de semi-clathrate de tétra-n-butyl ammonium comme frigoporteur diphasique - Etudes expérimentales et modélisation

Jérôme Douzet, Matthias Kwaterski, Alain Lallemand, Fabien Chauvy, Denis Flick, Jean-Michel Herri

Prototyping of a real size air-conditioning system using a tetra-*n*-butylammonium bromide semiclathrate hydrate slurry as secondary two-phase refrigerant – Experimental investigations and modelling

Jérôme Douzet[a], Matthias Kwaterski[a], Alain Lallemand[a], Fabien Chauvy[a], Denis Flick[b], Jean Michel Herri[a,*]

[a] École Nationale Supérieure des Mines de Saint-Etienne, Centre SPIN, département ProPICE, UMR CNRS 5307 Laboratoire Georges Friedel, 158 cours Fauriel, 42023 Saint-Etienne Cedex 02, France

[b] AgroParisTech, UMR 1145 Ingénierie Procédés Aliments, 16 rue Claude Bernard, 75231 Paris Cedex 05, France

* Corresponding author. Tel.: +33 477420292; fax: +33 477499692

E-mail address: herri@emse.fr (J. M. Herri).

Abstract

Among innovative processes developed in the field of refrigeration systems, technologies are encountered which are based on the application of Phase Change Materials (PCM) for the storage and transportation of energy. PCM are often provided by means of slurries. In the air-conditioning system presented here, a slurry of semi-clathrate hydrate crystals based on Tetra-*n*-Butyl-Ammonium Bromide (TBAB) is used as secondary refrigerant. The production of the slurry can be smoothed over day and night. Upon storage, the slurry can be distributed to end users, and molten to recover the cooling capacity. By adaption of a standard refrigeration

technology, it is at first demonstrated that an air-conditioning system can be established by replacing the standard refrigeration fluid by a slurry of TBAB based semi-clathrate hydrate. Furthermore, the study attempts to model the settling of particles within the storage tank, aiming at gaining some insight in their complex migration processes obtained during the production and distribution steps.

Keywords: Air-conditioning; Technology transfer; Hydrate slurries; Phase Change Material; TBAB; Storage Modelling

Nomenclature

Latin symbols

$A_{s,\,tank}$	surface area of the tank (m^2)
C	number density of hydrate particles, i.e. number of hydrate particles per unit of volume (m^{-3})
c_p	specific heat capacity at constant pressure (J kg^{-1} K^{-1})
d	mean equivalent diameter of hydrate particles (m)
D_{eq}	equivalent diffusivity (m^2 s^{-1})
$\Delta_{dis}h_{hyd}$	specific heat of dissociation/melting of the semi-clathrate hydrate (also called the “latent heat” of hydrate melting) (J kg^{-1})
g	acceleration of gravity on an average height the earth’s surface (m s^{-2})
h	specific enthalpy (J kg^{-1})
$h_{insulation}$	global heat transfer coefficient (trough lateral insulation) (W m^{-2} K^{-1})
H	enthalpy, (J)

m	mass (kg)
$\dot{m}$	mass based flow-rate (kg s^{-1})
M	molar mass (kg mol^{-1})
p_{tank}	tank perimeter (m)
P	thermal power (W)
t	time (s)
T	thermodynamic temperature (K)
v	velocity (m s^{-1})
V	volume (m^3)
w	mass fraction (-)
$w_{w,\,free}$	liquid phase mass fraction of water in excess with respect to the congruent point ("free water") (-)
z	charge number (-)
Z	spatial coordinate indicating the height position in the storage tank (m)

Greek symbols

β_m^H	mass-based hydrate phase fraction, $\beta_m^H = m^H/(m^H + m^{Lw})$ (-)
β_V^H	volume-based hydrate phase fraction, $\beta_m^H = V^H/(V^H + V^{Lw})$ (-)
Δ	difference in general
ϑ	celsius temperature (°C)
λ_{eq}	equivalent thermal conductivity of the slurry (W m^{-1} K^{-1})
μ	dynamic viscosity (Pa s)
ν_w	hydration number (-)
ν	stoichiometric coefficient (-)

ρ	density (kg m^{-3})
0	initial condition

Subscripts

A	anion, here more specifically A ≡ Br^-
C	cation, here more specifically C ≡ $(n\text{-}C_4H_9)_4N^+$
cgr	conditions at congruent melting and dissociation point
dis	dissociation
ext	external
fus	fusion/melting
hyd	semi-clathrate hydrate compound based on tetra-*n*-butylammonium bromide, i.e. abbreviation for $(n\text{-}C_4H_9)_4NBr\cdot\nu_w H_2O$ where the hydration number can be 26 or 38, i.e., the index "hyd" can refer to type A and type B TBAB-semi-clathrate hydrate, depending on the context
inlet	referring to an inlet to the crystalliser
max	maximum value
outlet	referring to an outlet from the crystalliser
set	settling
sol	solution, here in particular the liquid aqueous solution of tetra-*n*-butylammonium bromide
TBAB	tetra-*n*-butylammonium bromide
w	water

w, free referring to ”free water“, the water being present in the liquid phase in excess to the stoichiometric composition of a hypothetical presence of a semi-clathrate hydrate phase in the liquid phase

Superscripts

–	indicating an arithmetically averaged quantity
°	pure component
H	hydrate phase, here more particularly a semi-clathrate hydrate phase
L	liquid phase
L_w	aqueous liquid phase
S	solid phase
V	vapour phase (concerning primary fluid)

1. Introduction

The increasingly widespread use of air-conditioning systems all over the world has a direct impact on the global energy demands with respect to both the overall average electricity consumption over the years and the fluctuations of the energy consumption between days and nights. A special domain of application concerns the air-conditioning of spaces requiring high cooling capacities. With regard to the European market in particular, the chillers possessing cooling powers in the ranges of (20-500) kW or (500-1200) kW are important in this context. Coolers with these specifications are typically used for the air-conditioning of large building, public rooms or industrial buildings.

The principle of techniques based on Phase Change Materials (PCM) consists in storing energy by using the change in enthalpy accompanying the corresponding phase transition and to subsequently distribute the PCM, upon which the phase change has been performed, on demand. In such a process, the energy is preferably stored during periods in which the energy needs are low, i.e. generally at nighttime. Later, when the cooling capacity is needed, usually in the daytime, the PCM is distributed in accordance with the special requirements of the end-users. In addition, the thermodynamic regime of air-conditioning machines can be optimised since the night-time is a more appropriate period for the operation of thermodynamic cycles due to its lower average outside temperature.

A further advantage of using a PCM over using a classical refrigerant only is the possibility of confining the primary cooling cycle (i.e., the complete unit containing all the compressors, valves, heat exchangers and other technical devices) and thus, the primary refrigerant fluid, in a single localised space. This space could e.g. be a machine room which is exclusively dedicated to the generation of the secondary heat exchange medium. By smoothing the electrical consumption over 24 hours, the cooling cycle, hereafter referred to as “primary loop”, can be optimised in order to allow the decrease of the total amount of primary refrigerants, and hence diminishes their ecological impact. In this context, especially the refrigerants being subject to the Montreal and Kyoto Protocols are to be mentioned. The “cold” is distributed to the end-user via a secondary loop in which the PCM is directly conducted in the form of a slurry. Alternatively, the energy removal in this type of cycles is carried out by using another liquid heat exchange medium, e. g. water. In the latter case, this third heat exchange medium would be used in a tertiary cycle being brought in heat conducting (diathermal) contact with the secondary PCM based cooling cycle. The PCM would in that event remain in the machine room as well.

Phase change materials based on ice slurries have been developed by several companies for applications in the domain of refrigeration, i.e., for cooling at Celsius temperatures below zero. They benefit from the large enthalpy of fusion due to the breakup of the hydrogen bonds between the water molecules. In those types of refrigeration plants, water is used as cooling medium, which is crystallised in the form of ice. The melting point and, hence, the operation temperature can be lowered by adding appropriate additives, such as alcohols. Different types of ice slurry generators have been developed (Meunier et al., 2007). Those ones holding a significant market share are the scraped surface heat exchangers, as for example the Sunwell system (Gibert, 2006) or, like in this work, the Heatcraft generator (Compingt et al., 2009).

However, for applications above 0°C, such as for air-conditioning, the use of ice slurries is no longer applicable: the melting point of ice can not be shifted to positive Celsius temperatures. Several authors (Lipkowski et al., 2002; Obata, et al. 2003; Oyama et al., 2005) have shown that semi-clathrate hydrates formed by certain quaternary ammonium salts can be used as PCM for air-conditioning applications. In fact, these solid compounds possess melting temperatures above 0°C, and, due to their crystallographic structure, which is based on a H-bonded framework, the values of their dissociation enthalpies are relatively high.

The deployment of the technology needs to be accompanied with a fundamental understanding of the behaviour of the slurry in the different steps of the overall process. To achieve this aim, it is required to not only investigate the generation of the slurry in the crystalliser, but also its storage in the tank as well as its distribution over the various loops as function of time. Studies on the heat transfer rates in processes using TBAB based semi-clathrate hydrate slurries have been conducted for different experimental/technical

configurations. In particular, results on the heat transfer in pipes (Wenji et al, 2009; Ma et al., 2010; Kumano et al., 2011b) or on the heat transfer in plate heat exchangers (Ma and Zhang, 2011) have been published. The distribution of the slurry in particular plants has been investigated by means of rheological studies (Darbouret et al., 2005b), studies on the flow characteristics (Kumano et al., 2011a) and pressure drop experiments in pipes (Ma and Zhang, 2012).

In the present work, we focus on the storage tank which is the location where the settling of the hydrate particles takes place. A numerical model is proposed to predict the evolution of the hydrate content within the plant in both time and space as well as to estimate the overall storage cooling capacity. The model takes into account the natural settling of the hydrate crystals as function of their density. Furthermore, the storage tank is subjected to fluid circulations with both the crystalliser and the end-user units which disturb the settling.

2. Methods and Materials

2.1. Principle of the air-conditioning system using a TBAB semi-clathrate hydrate slurry

Zhang et al. (2009) have presented a literature survey on several PCM. Tetra-*n*-butyl ammonium bromide (TBAB), in the form of an aqueous solution, is an appropriate candidate because of its availability at a moderate price, and the relative high melting temperature (up to 12.4°C) and rather large heat of dissociation of the corresponding semi-clathrate hydrates which can be formed. Indeed, together with water molecules in aqueous solution, TBAB is

able to generate crystals of semi-clathrate hydrate compounds which are formed according to the reverse reaction of the general dissociation equilibrium

$$\mathrm{C}_{\nu_\mathrm{C}}\mathrm{A}_{\nu_\mathrm{A}} \cdot \nu_\mathrm{w}\mathrm{H_2O}\,(\mathrm{S=H}) = \nu_\mathrm{w}\mathrm{H_2O}\,(\mathrm{L_w}) + \nu_\mathrm{C}\mathrm{C}^{z_\mathrm{C}+}(\mathrm{L_w}) + \nu_\mathrm{A}\mathrm{A}^{|z_\mathrm{A}|-}(\mathrm{L_w}) \qquad (1)$$

In the particular case of TBAB with C ≡ (n-C_4H_9)$_4N^+$ and A ≡ Br^- considered here, the stoichiometric coefficients ν_C and ν_A as well as the charge numbers z_C and $|z_\mathrm{A}|$ of the corresponding ions are unity. Different numerical values have been reported in the literature for ν_w, the stoichiometric coefficient of water. This quantity ν_w, when related to one stoichiometric unit of the salt also referred to as the hydration number, corresponds to a given semi-clathrate hydrate compound. Whereas Dyadin and Udachin (Dyadin and Udachin, 1984) for example report four different semi-clathrate hydrates of hydration numbers ν_w = 24, 26, 32, 36, Shimada and co-workers (Shimada et al., 2005) found only two kinds of hydrates, referred to as type A and B, respectively, with ν_w = 26 and 38.

When dispersed in the surrounding liquid aqueous solution phase, the semi-clathrate hydrate crystals form a slurry that can be used as a PCM according to formation/dissociation equilibrium defined in Eq. (1). The structure of these compounds is similar to the structure of ice. Hence, when being used as a semi-clathrate hydrate slurry in cold storage applications, in an analogue way as in the case of an ice slurry, the storage is based on making use of the energy of the hydrogen bonds between the water molecules. However, in contrast to the lattice structure of ice, the presence of the quaternary ammonium allows for stabilising the three-dimensional molecular network at a temperature superior than 0 °C (Shimada et al., 2005). In Fig. 1 the crystallisation temperature at equilibrium is plotted as function of the mass fraction of TBAB at 0.1 MPa. The two curves correspond to the two different modifications of semi-clathrate hydrates mentioned above with hydration numbers of ν_w = 26

and 38, respectively, as they have been described by Shimada et al. (Shimada et al., 2005). The authors have named the compounds semi-clathrate hydrates of type A and B, respectively. The specific enthalpy of dissociation $\Delta_{dis}h_{hyd}$ according to the reaction described by Eq. (1) amounts to about 193 kJ kg^{-1} for the semi-clathrate hydrate of type A, and 200 kJ kg^{-1} for the hydrate of type B, respectively (Obata et al., 2003; Oyama et al., 2005).

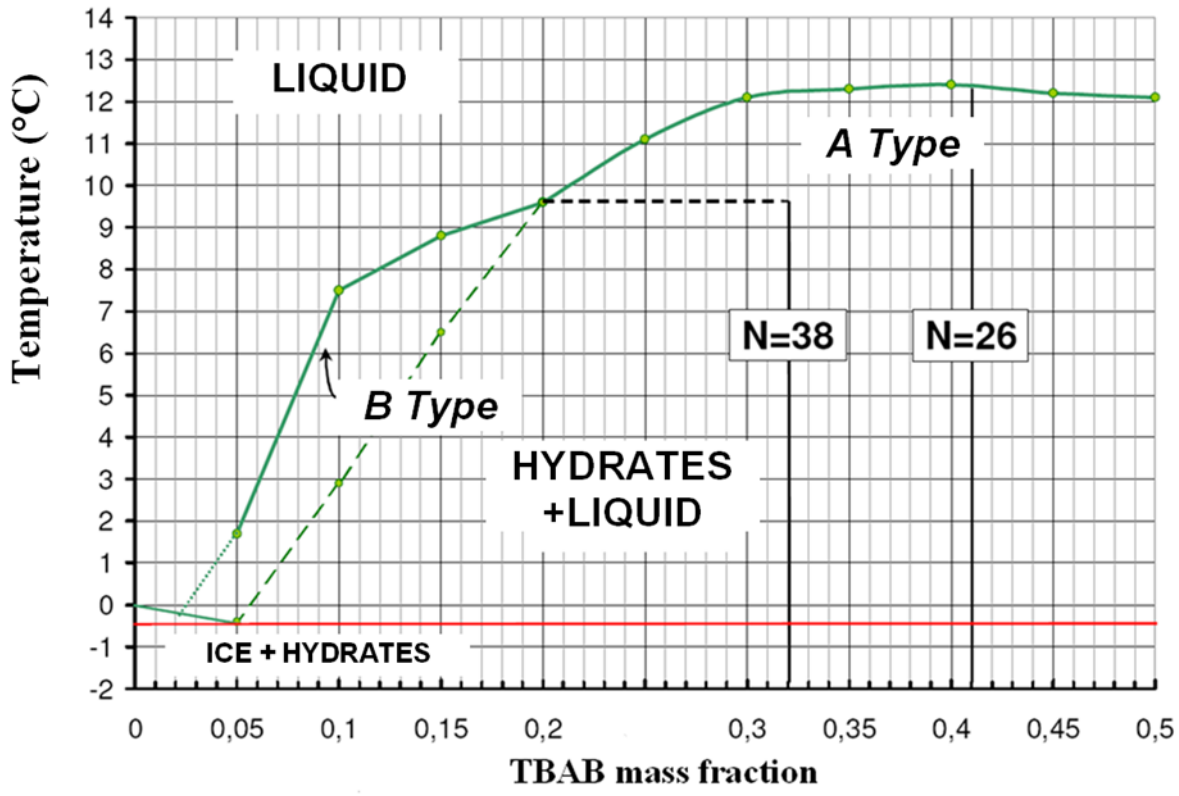

Fig. 1 H-L_w Phase diagram of TBAB hydrates at ambient pressure (Darbouret, 2005a).

In Table 1, the cooling capacities of a given mass of two cooling medias liquid water and TBAB semi-clathrate hydrate slurries, are compared in terms of their corresponding enthalpy change $\overline{\Delta H}$. In the left two columns of Table 1 data on the average change in enthalpy $\overline{\Delta H}$ for generating a temperature change ΔT of 4 K and 6 K, respectively, in a mass of $m_w^{L_w}$ of chilled water are listed. The water possesses an initial temperature ϑ_0 between 4 °C and 8 °C,

which is typical for air-conditioning systems. These data are compared in the following three columns to data on the corresponding enthalpy changes that 1 kg of a TBAB semi-clathtrate hydrate slurry of different mass based hydrate phase fractions of 10 %, 20 % and 30 % undergoes. Thereby, the mass based phase fraction β_m^{H} of the semi-clathrate hydrate phase is defined according to:

$$\beta_m^{\mathrm{H}} = \frac{m^{\mathrm{H}}}{m^{\mathrm{H}} + m^{\mathrm{L_w}}} \qquad (2)$$

where m^{H} refers to the mass of the semi-clathrate hydrate phase and $m^{\mathrm{L_w}}$ for the mass of the liquid aqueous solution phase in the slurry. Whereas m^{H} does ideally refer to a pure phase, the semi-clathrate hydrate compound, when according to Eq. (1) only a single semi-clathrate of fixed hydration number ν_{w} is formed (i.e., $m^{\mathrm{H}} \equiv m_{\mathrm{hyd}}^{\mathrm{H}}$, where the index "hyd" is an abbreviation for "(n-$C_4H_9)_4$N Br$\cdot \nu_{\mathrm{w}}$ H_2O"), the liquid phase consists of the aqueous TBAB solution (i.e. $m^{\mathrm{L_w}} \equiv m_{\mathrm{sol}}^{\mathrm{L_w}}$, where the index "sol" is an abbreviation for the aqueous binary solution of TBAB). It has to be remarked that although the initial temperatures of the two different cooling media are in the same region, the nature of the enthalpy change is different. For chilled water, the enthalpy change leads to a change in temperature but not to a phase transition. Hence, the averaged quantity $\overline{\Delta H}$ corresponds to what is referred to as "sensible heat" and is expressed by:

$$\overline{\Delta H} \approx m_{\mathrm{w}}^{\mathrm{L_w}} \bar{c}_{p,\mathrm{w}}^{\circ,\mathrm{L_w}} \Delta T \qquad (3)$$

where $m_{\mathrm{w}}^{\mathrm{L_w}}$ is the mass of the portion of liquid water, $\bar{c}_{p,\mathrm{w}}^{\circ,\mathrm{L_w}}$ the average specific isobaric heat capacity of pure liquid water at a Celsius temperature around the reference temperature ϑ_0 and ΔT the temperature change accompanying the average enthalpy change $\overline{\Delta H}$. In contrast, the average enthalpy change experienced by the hydrate slurry, correspond to $\overline{\Delta H}$-values that describe the simultaneous phase change and chemical dissociation reaction of the semi-

clathrate hydrate according to Eq. (1). In other words, this quantity, also called “latent heat”, is given by:

$$\overline{\Delta H} \approx m_{\mathrm{hyd}}^{\mathrm{H}} \Delta_{\mathrm{dis}} h_{\mathrm{hyd}} = \beta_m^{\mathrm{H}} \left(m_{\mathrm{hyd}}^{\mathrm{H}} + m_{\mathrm{sol}}^{\mathrm{L_W}} \right) \Delta_{\mathrm{dis}} h_{\mathrm{hyd}} \quad (4)$$

where $\Delta_{\mathrm{dis}} h_{\mathrm{hyd}}$ stands for the specific enthalpy of dissociation at the dissociation temperature and at ambient pressure. Eq. (4) illustrates, that the $\overline{\Delta H}$ -values compiled in Table 1 for the hydrate slurry as cooling medium do not include the contribution arising from the sensible heat, but do instead only take into account the contribution from the combined phase and chemical equilibrium described by Eq. (1). For air-conditioning systems based on the use of chilled water, it becomes clear from Table 1 that for a portion of water of mass $m_{\mathrm{w}}^{\mathrm{L_w}}$ = 1 kg and an increase in temperature of 5 °C, the corresponding change in enthalpy amounts to about 20 kJ kg^{-1}. In contrast, the same portion of mass $m_{\text{hyd-slurry}} = m_{\mathrm{hyd}}^{\mathrm{H}} + m_{\mathrm{sol}}^{\mathrm{L_w}}$ = 1 kg of a slurry based on $\beta_{\mathrm{m}}^{\mathrm{H}}$ = 20 % of TBAB semi-clathrate hydrates, is capable of providing an enthalpy change which is twice the value obtained for the previous case of chilled water. This is particularly remarkable if it is realised that for the evaluation of the cooling potential of the slurry only the effect of the dissociation the semi-clathrate hydrates (“latent heat” of the solid phase) has been considered here.

Table 1 Comparison between the average enthalpy changes $\overline{\Delta H}$ undergone by 1 kg of chilled liquid water and 1 kg of TBAB based hydrate slurries at $\vartheta_0 \in [4,8]\,°\mathrm{C}$

	$m_{\mathrm{w}}^{\circ,\mathrm{L_w}} = 1\,\mathrm{kg}$ of chilled water at $\vartheta_0 \in [4,8]\,°\mathrm{C}$ experiencing a temperature change ΔT of		$m_{\text{hyd-slurry}} = 1\,\mathrm{kg}$ of TBAB semi-clathrate hydrates slurries with mass based hydrate phase fractions β_m^{H} of		
	4 K	6 K	10 %	20 %	30%
$\overline{\Delta H}/\mathrm{kJ}$	17	25	20	40	60

The densities amount to 1080 kg m^{-3} for the hydrate crystals of type A and 1070 kg m^{-3} for the hydrate crystals of B, respectively (Oyama et al., 2005). At temperatures in the interval of 10 °C and 24 °C and for a TBAB mass fraction in the aqueous liquid phase between 0.2 and 0.4, the corresponding density of the aqueous solution of TBAB varies from 1021 kg m^{-3} to 1039 kg m^{-3} (Darbouret, 2005a; Obata et al., 2003; Belandria et al., 2009). As a result, the hydrate particles use to sink down in the aqueous solution and can settle at the bottom of the reactor. Therefore, the slurry can become inhomogeneous, especially in non-stirred zones. This phenomenon needs to be taken into account when designing the apparatus, particularly with regard to the storage tank.

2.2. Technological description of the installation

We have built and instrumented our own prototype by adapting a technology designed for ice slurries and available, on the European market, from the company Heatcraft-Europe. However, in this prototype plant, the PCM fluid has been exchanged for a tetra-*n*-butyl ammonium bromide (TBAB) aqueous solution. This technology is comparable to the one developed and commercialised by JFE Engineering Corporation, Japan (Takao et al., 2001; Takao et al., 2004; Mizukami, 2010, Ogoshi et al., 2010). The first prototype of JFE Engineering Corporation was built in 2005 and to this day, approximately 10 systems with a cooling capacity of up to 2 MW have been sold. In general, the Japanese company has transformed a traditional air-conditioning system by using cold water storage tanks and several intermediates loops and fluids (up to 4) (Ogoshi et al., 2010).

The flowsheet of the prototype constructed in our group is shown in Fig. 2. First of all, the experimental setup is composed of a primary and a generation loop. After, in the utilisation

loop, the slurry is distributed to the end-user. The capacity of the installation corresponds to the capability to provide the air-conditioning for four rooms located on three different floors (total surface area of approximately 145 m²).

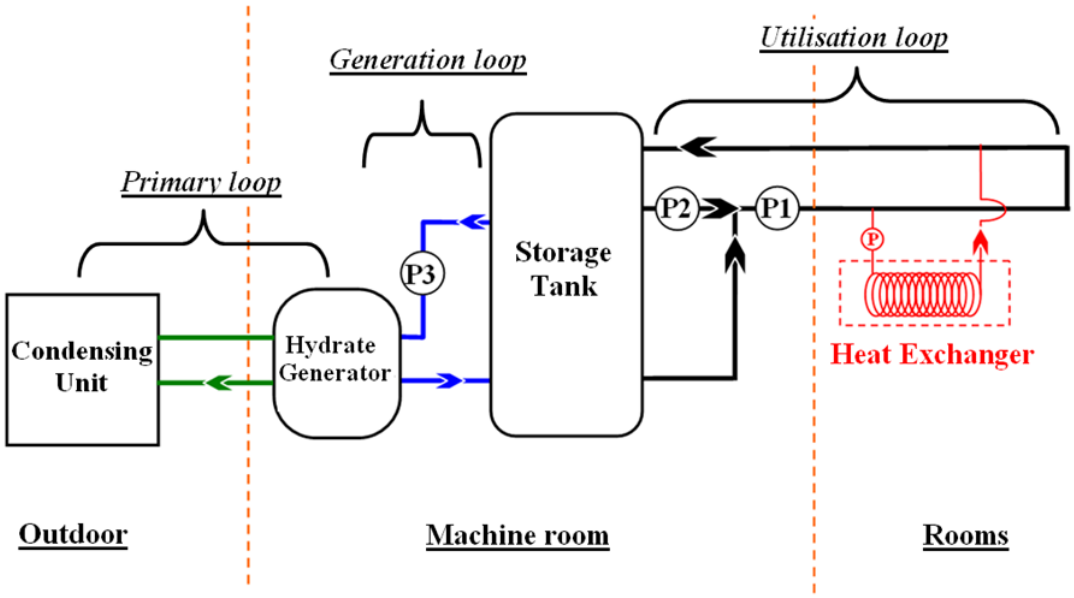

Fig. 2 Basic scheme of the (full size) complete/overall installation.

The primary loop is a classical cooling cycle composed of a compression, condensation, expansion and evaporation stage/unit, respectively, of a primary cooling fluid (refrigerant). In the current unit, the HydroFluoroCarbon (HFC) R407C is used for that purpose. The condensing unit (Scroll compressor + condenser) is located outside the building to liquefy R407C at elevated pressure (around 1 MPa) and ambient temperature. The aqueous solution of TBAB is crystallised in the hydrate generator by removing energy in the form of heat by means of the evaporating R407C fluid. The condensing unit is a standard model from LENNOX ® with a cooling capacity of 29.3 kW (electric power consumption of 13.8 kW).

After passing through the expansion valve, the R407C fluid enters the heat exchanger of the hydrate generator, a schematic representation of which is depicted in Fig. 3. The heat

exchanger is composed of five plates constituting an internal flow loop in which the R407C is evaporated. The temperature is controlled on both sides of the five plates, respectively, which in turn are in direct contact with the TBAB solution. On the surface of each of the two sides of the plates the liquid solution undergoes a phase transition to the solid state and hence, is partially converted into semi-clathrate hydrate. As a result, the hydrate generator is composed of 6 parallel connected stages separated by 5 exchanger plates. Each stage is sized for a cooling capacity of about 5 kW to 6 kW in the original refrigeration application (by using R404A as primary heat exchange fluid and ice slurries as secondary cooling medium). The semi-clathrate hydrate crystals tend to accumulate and stick on the surface of the plates, from where they are taken off by rotating scrappers. This technology, further details of which can be found in literature (Ben Lakhdar and Melinder, 2002; Ben Lakhdar et al., 2005; Compingt et al., 2009), is supplied by the company HeatCraft (Genas, France). At a height of 0.75 m and a diameter of about 1 m, the hydrate generator possesses an internal volume of 0.2 m^3.

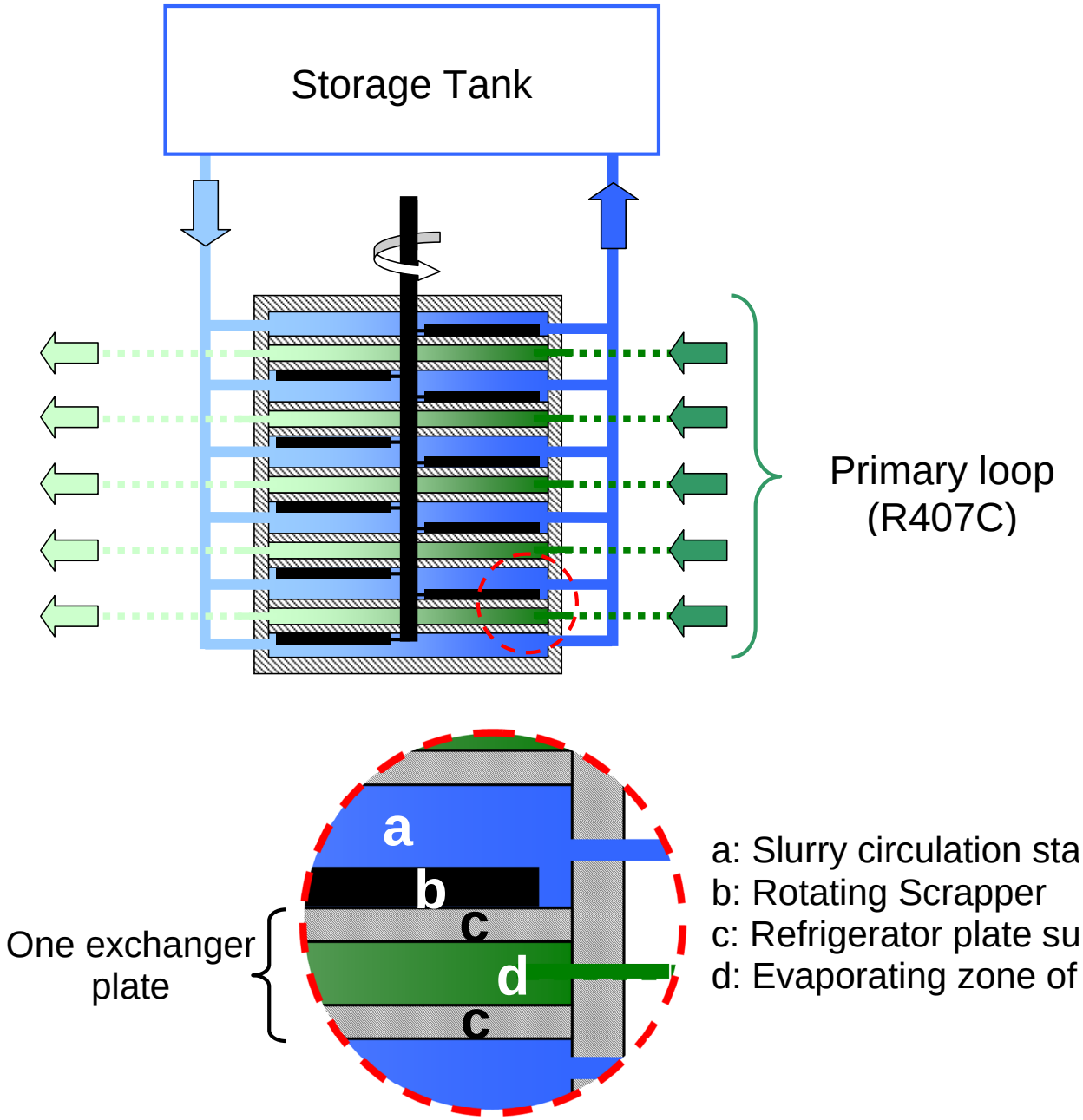

Fig. 3 Schematic representation of the hydrate generating unit.

The storage tank and the hydrate generator are connected via a so-called generation loop. The liquid solution is sucked at the top of the storage tank where the mass-based hydrate phase fraction is lower. Since the density of the hydrate particles is slightly higher than the density

of the residual liquid solution, the solid particles tend to settle in the tank, especially if the slurry is unstirred. The tendency is that the liquid phase (or, more precisely, a suspension with lower hydrate phase fraction) is accumulated at the top of the tank whereas the crystals sediment at the bottom, leading to a slurry with higher hydrate phase fraction. The tank used in our experimental setup is 2.5 m height and possesses volume of about 2 m^3. It is entirely made of stainless steel and insulated with a nitrile rubber jacket/coating of 19 mm thickness. The storage tank is filled with a 39 wt% TBAB aqueous solution, which is close to the concentration at the congruent melting and dissociation point of the type A TBAB semi-clathrate hydrate at $w_{\mathrm{TBAB,\,cgr}}$ = 40.77 %, where the corresponding phase transition temperature amounts to $\vartheta_{\mathrm{hyd,\,fus,\,cgr}} = \vartheta_{\mathrm{hyd,\,dis,\,cgr}}$ = 12.4 °C (Darbouret, 2005a) as can be seen in Fig. 1.

The secondary flow loop is the network to distribute the slurry to the end-user. The slurry is sucked from two different levels of the storage tank. The volumetric pump P1 (Fig. 4) provides the flow and maintains the flow-rate in the loop by sucking the slurry at the bottom of the storage tank. At this level the phase fraction of semi-clathrate hydrates can attain the greatest values of up to (40-50) wt%. Due to the high solid phase fraction, the semi-clathrate hydrate slurry possesses the relatively greatest cooling capacity at the bottom of the tank. For that reason, it is very important that a significant portion of the hydrate suspension used for the secondary cycle is withdrawn at that location. However, at such a solid fraction, the viscosity is too high for the slurry to be treated by the pump without difficulties. Therefore, the solid phase fraction needs to be reduced to a value of (20-30) wt% to end up at a reasonable viscosity (Darbouret, 2005a). The slurry is diluted by using another pump P2 which sucks the remaining portion of liquid for the secondary cycle or, more precisely, a slurry of lower hydrate phase fraction, at the top of the storage tank. The stream originating from this exit is combined with the bottom stream just in front of the position at which the

pump P1 is located (Fig. 4). Thus, the pump P2 serves as a means that allows particularly for controlling the volume fraction of the solid particles in the secondary loop. In practice, the flow rate of P2 is regulated in such a way that it does not exceed the flowrate imposed by P1. With regard to the material, this loop is made of cooper brass pipes of 40 mm internal diameter and a length of approximately 100 m. It distributes the slurry to the rooms to be air-conditioned.

The characteristics of the pumps are as follows. Pump P1 is a lobes pump of type TLS 1-40 provided by INOXPA which possesses a nominal power of 1.1 kW and a maximum flow-rate of 8 $m^3 h^{-1}$. Pump P2 is a centrifugal pump from INOXPA, model ESTAMPINOX EFI 2003, with a power of 0.37 kW and a measured flow-rate at 30 Hz of 3 $m^3 h^{-1}$. Pump P3 is a lobes pump from INOXPA of type TLS 3-50 having a 3 kW power output and a maximum flow-rate of 30 $m^3 h^{-1}$.

The end-user fan coils implemented in the setup are standard model heat exchangers from LENNOX ®. They are connected to the distribution flow loop via brass pipes of 10 mm internal diameter. A small pump HXL 63-15P provided by SALMSON, is installed in each of the supply lines of the corresponding fan coils. The fan coils cool down the room by melting the hydrate slurry. Three floors have been air-conditioned through a total of 7 fan coils. Whereas the 1st floor has been air-conditioned by means of three fan coils, the 2nd and 3rd floor are equipped with two fan coils each. One of these exchangers is additionally endowed with temperature sensors (Fig. 4).

2.3. Instrumentation

A schematic representation of the experimental setup in the form of a flow sheet diagram is shown in Fig. 4.

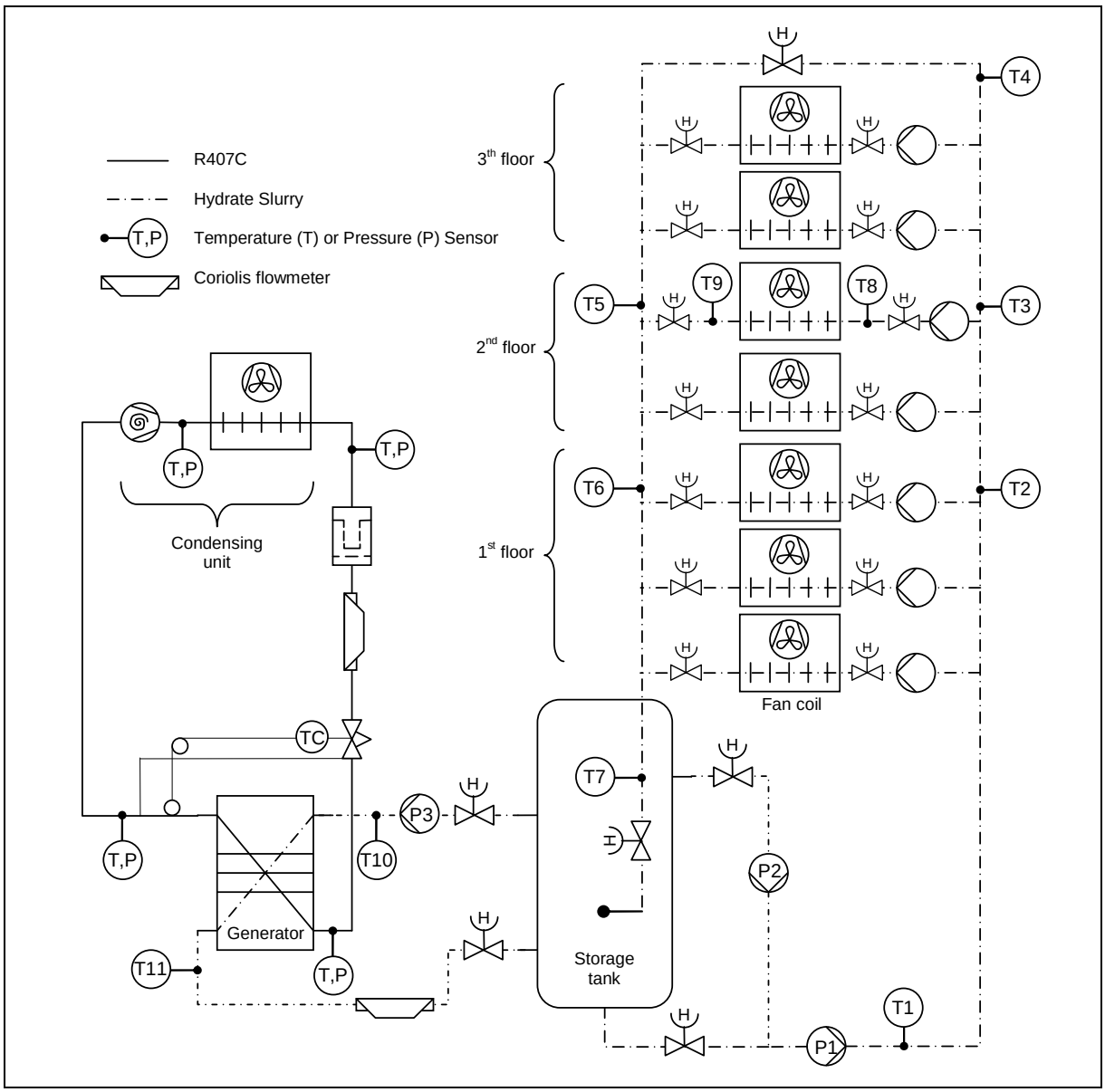

Fig. 4 Scheme of the full size installation, including in particular the locations of the sensors.

To measure and control the temperature, Pt100 type temperature sensors have been used. The sensors are screwed on brass connectors which in turn are brazed on the cooper pipes. The sensor tip is located in the pipe. The pressure transducers are piezo-resistive transmitters provided by KELLER. They are fixed to the pipe in the same way as the temperature sensors

and serve as devices for monitoring the pressure in the primary loop and thereby for characterizing the state of the R407C. In order to measure the flow rate, two Coriolis flow-meters from MICRO MOTION have been installed. The first one is placed in the primary loop, whereas the second one is incorporated in the generation loop. The location of the last mentioned flow meter can be changed allowing for incorporating it into the utilisation loop.

2.4. General design of the installation

The PCM slurries can be stored which allows for producing the cold energy during the night. Therefore the size of the cooling machines can be reduced. As a consequence of this, the plant can be run continuously, at a constant rate, instead of working only during the peak demand. Moreover, the average outdoor temperature is lower at night-time than in the daytime which leads to a better energetic balance of thermodynamic machines. Finally, depending on the local policies, the electricity could also be available at a lower price during night than during the day. Fig. 5 plots the histogram of the cooling capacity of a typical air-conditioning plant designed for cooling a room of 145 m^2 with the peak of cooling demand during the day. The energy need can be managed by storing the slurry during the night and melting it in the daytime.

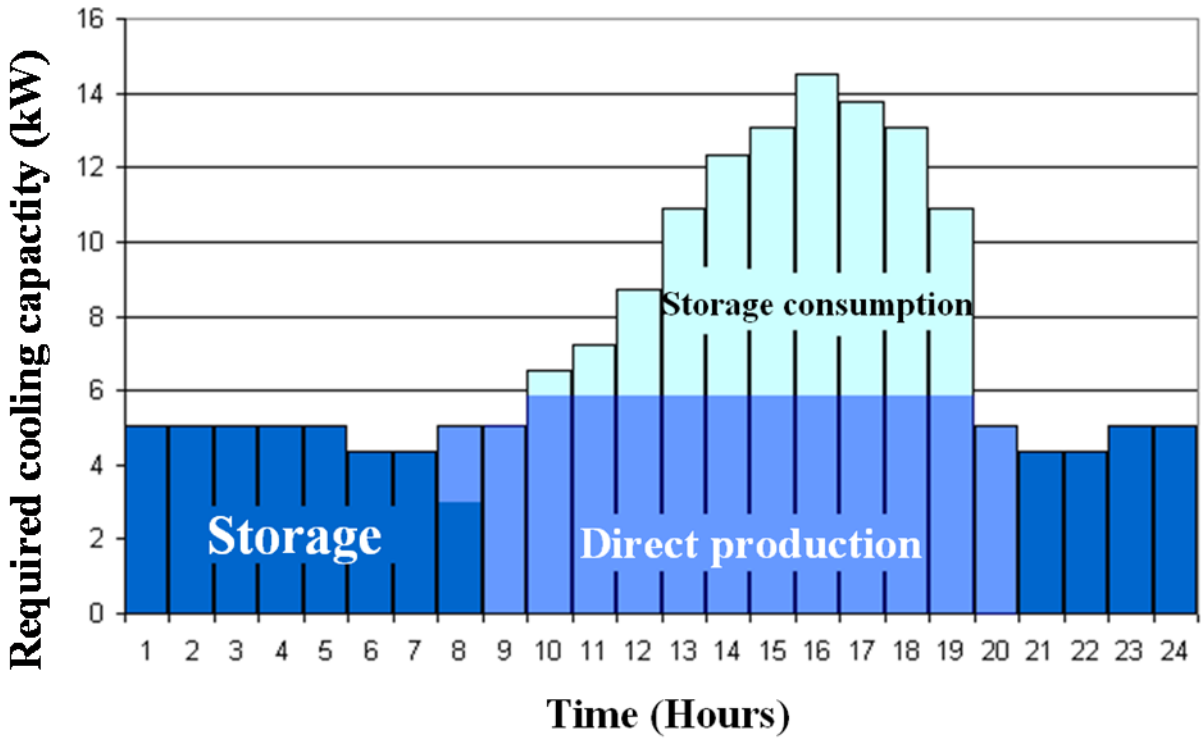

Fig. 5 Histogram of the management of the air-conditioning cooling capacities by using energy storage (Dumas, 2002).

Our prototype has a storage tank of 2 m^3. If the tank is homogeneously filled with a TBAB semi-clathrate hydrate slurry containing 30 wt% of solid phase, it is able to store a cooling capacity of 29 kWh. This allows for supplying a cooling capacity of 14.5 kW during approximately 2 hours.

3. Modelling

3.1. Objectives

Since experimental investigations on the different processes going on in the plant are very time consuming, only a limited number of technical configurations and parametric conditions can be studied experimentally. For example, liquid phase and overall TBAB concentration, specific operating conditions as for instance of temperature, pressure or flowrates, or the geometry of the tank and the location of the tank inlets and outlets, to name but a few are experimentally accessible. However, as outlined above, due to the tediousness of measurements, a modelling approach has been developed to simulate a large number of configurations of our air-conditioning plant. The main hypotheses and the constitutive equations of the model are presented in more detail below.

One of the crucial phenomena having a great impact on the overall process in our plant is the settling of the semi-clathrate hydrate particles inside the storage tank. Since the density of the hydrate crystals does exceed the density of the liquid solution, a gradient in hydrate phase fraction is established within the slurry inside the tank. The hydrate phase tends to accumulate at the bottom of the tank. The experiments are conducted close to the composition at the congruent melting point. Thus, the composition of the liquid solution assumes practically the value which corresponds to the stoichiometric ratio of the components present in the type A semi-clathrate hydrate compound. Due to the value of the initial overall composition chosen for preparing the binary $\{H_2O + TBAB\}$ mixture, the concentration of TBAB in the liquid phase varies only a little during the generation and the dissociation of the slurry, respectively. As a further consequence of the choice of the initial overall TBAB concentration, the temperature remains quasi-constant. In future experiments it could be interesting to use a lower concentration of TBAB. Thereby, the process would be forced to operate in a lower temperature region due to the composition dependence of the dissociation temperature of the

semi-clathrate hydrate compound. In other words, both the temperature and TBAB concentration would vary during the crystallisation as can be verified in Fig. 1.

The model has been developed in order to predict the hydrodynamic behaviour and thermo-physical properties of the hydrate slurries in the storage tank. It aims at predicting the evolution of the hydrate content in space (as function of the tank geometry and in particular the positions of the inlet and outlet pipes) and time, and as function of the operating conditions (generation in the crystalliser on the one hand and utilisation by end-users on the other hand). The local variables the model calculations are based upon are the hydrate fraction, the temperature, the composition of the residual liquid solution and the mean diameter of the hydrate crystals.

3.2. Main model hypotheses

With regard to the storage tank, it is assumed that the problem can be treated by assuming a 1D geometry. More specifically, the different types of motions occurring in the liquid solution, as e.g. the settling of hydrate particles, are considered as movements along the vertical axis of the cylindrical reactor. This assumption implies that the slurry is considered to be homogeneous at a given horizontal cross section.

The overall volume of the slurry is considered as constant. On the other hand, at the congruent melting and dissociation point of the semi-clathrate hydrate, the molar volumes of the two phases in equilibrium are constant. Thus, they are particularly independent of the relative amounts of the two phases present in the reactor. Satisfying the aforementioned condition of a constant overall slurry volume would therefore be equivalent with requiring additionally that

the molar volumes of the liquid and semi-clathrate hydrate phase be equal. Obviously, this condition is generally and in the particular case treated here not fulfilled and, hence, the existence of such ideal slurry is just hypothetical. Therefore, the volume variations occurring in the slurry due to melting or crystallisation are neglected. In fact, the relative difference in density between the solid and the liquid phase amounts to only around 5 %. For an average solid phase fraction of 40 wt%, the total volume variation is estimated to be less than 2 %.

The buoyancy forces which depend on the difference in the densities of the two phases, are taken into account in the settling law, via a modified Stokes equation (Eq. (7)). The time constants for the generation and utilisation loops are neglected. In other words the volume of slurry in each loop, respectively 0.2 m^3 and 0.1 m^3, is neglected in comparison with the volume of slurry contained in the tank, which is approximately 2 m^3. As a consequence, the time necessary for the slurry to flow from the inlet to the outlet of each loop is supposed to be zero.

3.3. Constitutive model equations

The mean velocity of the slurry v at a given height in the storage tank can be calculated from the flow-rates obtained in the generation and utilisation loop, respectively, and can be expressed as function of the volume based hydrate phase fraction β_V^{H}, and the velocities of the residual liquid solution and the semi-clathrate hydrate, respectively, named v_{sol} and v_{hyd} according to

$$\left(1-\beta_V^{\mathrm{H}}\right)v_{\mathrm{sol}} + \beta_V^{\mathrm{H}} v_{\mathrm{hyd}} = v \qquad (5)$$

In Eq. (5), β_V^{H} is defined by analogy with β_m^{H} in Eq. (2) according to

$$\beta_V^{\mathrm{H}} = \frac{V^{\mathrm{H}}}{V^{\mathrm{H}} + V^{\mathrm{L_w}}} \qquad (6)$$

where V^{H} and $V^{\mathrm{L_w}}$ are the volumes of the semi-clathrate hydrate and the solution phase, respectively.

The settling can be described by a modified version of Stokes' law, i.e., the settling process can be represented by assuming that the hydrate crystals are of spherical geometry characterised by an the equivalent particle diameter. For high hydrate phase fractions, the settling is damped with a sigmoid damping function $f(\beta_V^{\mathrm{H}})$, which does assume the upper limiting value of unity, i.e. $f(\beta_V^{\mathrm{H}}) = 1$, when $\beta_V^{\mathrm{H}} = 0$ and values close to 0 when β_V^{H} approaches its maximum value $\beta_{V,\max}^{\mathrm{H}}$. Thus, the equation describing the settling velocity v_{set} in terms of difference in the densities of the solution ρ_{sol} and the hydrate particle ρ_{hyd}, the diameter of the particle *d*, the dynamic viscosity μ_{sol} of the residual liquid solution, and the damping function $f(\beta_V^{\mathrm{H}} - \beta_{V,\max}^{\mathrm{H}})$, respectively, is given by:

$$v_{\mathrm{set}} = \frac{g\left(\rho_{\mathrm{sol}} - \rho_{\mathrm{hyd}}\right)d^2}{18\mu_{\mathrm{sol}}} f\left(\beta_V^{\mathrm{H}} - \beta_{V,\max}^{\mathrm{H}}\right) \qquad (7)$$

The maximum value of β_V^{H} is evaluated to be close to 0.74 or 0.52, depending on the organisation of the sedimented crystal particles. For estimating $\beta_{V,\max}^{\mathrm{H}}$, Darbouret et al. (2005a) assumed that the particles of A type semi-clathrate hydrate settle in such a way that they are arranged geometrically as a close-packed sphere packing, as it is e.g. achieved for spheres in a face-centred cubic lattice. This close-packed sphere packing corresponds to a value of 0.74 for $\beta_{V,\max}^{\mathrm{H}}$. For type B hydrate, the authors assumed a threshold of $\beta_{V,\max}^{\mathrm{H}} = 0.52$ which is the $\beta_{V,\max}^{\mathrm{H}}$-value observed for the close packing of spheres in a simple cubic lattice. Finally it is assumed that the semi-clathrate hydrate particles do not agglomerate to form

clusters which would settle more rapidly. The viscosity μ_{sol} of the TBAB solution has been measured as function of temperature and TBAB mass fraction. The value used in the model calculations will be given in Table 2 (see section 4.4). Whereas the hydrate density ρ_{hyd} at the given temperature is regarded as constant, the density of the liquid solution ρ_{sol} depends besides temperature on its composition (Darbouret 2005a).The value for the density of type A semi-clathrate hydrate of 1080 kg m^{-3} was taken from Oyama et al. (2005). For the liquid phase density, a correlation has been performed on the results as published by Darbouret (2005a) of ρ_{sol} and the corresponding weight fractions $w_{TBAB}^{L_w}$. The latter provided data on ρ_{sol} of the liquid solution phase as function of the equilibrium temperature (and the corresponding weight fraction $w_{TBAB}^{L_w}$, respectively) of mixtures on the H-L_w coexisting curve. The settling velocity v_{set} is related to the velocities of the residual TBAB solution v_{sol} and the semi-clathrate hydrate crystals v_{hyd}, respectively, by the following equation

$$v_{set} = v_{sol} - v_{hyd} \qquad (8)$$

All the hydrate crystals at a given height grow or melt simultaneously. In other words, except from their formation in the generation loop or their dissociation in the utilisation loop, they do not appear or disappear. The number of hydrate particles per unit of volume is noted *C*. The effect of the particle size distribution (in terms of the diameter around its mean value) on the settling of the semi-clathrate hydrate crystals (settling velocity being smaller for smaller particles) is taken into account by an equivalent hydrate diffusivity $D_{eq.hyd}$, which is to be adjusted to experimental results. Time and height position in the tank are denoted as *t* and *Z*, respectively. Thus, the material balance for the hydrate crystals is to be expressed by

$$\frac{\partial C}{\partial t} + \frac{\partial}{\partial Z}\left(C v_{hyd} - D_{eq.hyd} \frac{\partial C}{\partial Z} \right) = 0 \qquad (9)$$

With regard to the enthalpy balance, only the latent heat corresponding to the simultaneous processes of dissociation and melting of the semi-clathrate hydrate, $\Delta_{\mathrm{dis}} h_{\mathrm{hyd}}$, is taken into account. Thus, the enthalpy per unit volume of the slurry is given by $\beta_V^{\mathrm{H}} \rho_{\mathrm{hyd}} \Delta_{\mathrm{dis}} h_{\mathrm{hyd}}$. The hydrate particles can melt inside the tank due to lateral heat losses or due to the fact that they move towards warmer regions (decrease of hydrates diameter). The equation used for calculating the hydrate phase fraction β_V^{H} reads

$$-\frac{\partial}{\partial t}\left(A_{\mathrm{s,\,tank}} \beta_V^{\mathrm{H}} \rho_{\mathrm{hyd}} \Delta_{\mathrm{dis}} h_{\mathrm{hyd}}\right) + \frac{\partial}{\partial Z}\left\{A_{\mathrm{s,\,tank}}\left[\rho_{\mathrm{hyd}} \Delta_{\mathrm{dis}} h_{\mathrm{hyd}}\left(D_{\mathrm{eq,\,hyd}} \frac{\partial \beta_V^{\mathrm{H}}}{\partial Z} - \beta_V^{\mathrm{H}} \nu_{\mathrm{hyd}}\right) - \lambda_{\mathrm{eq}} \frac{\partial T}{\partial Z}\right]\right\} \quad (10)$$
$$= h_{\mathrm{insulation}}\, p_{\mathrm{tank}} \left(T_{\mathrm{ext}} - T\right)$$

where $A_{\mathrm{s,\,tank}}$ is the tank surface area, p_{tank} its perimeter, λ_{eq} the equivalent thermal conductivity of the hydrate slurry and $h_{\mathrm{insulation}}$ the global heat transfer coefficient (trough the lateral insulation of the tank). T_{ext} is the external temperature, i.e. the temperature of the room where the tank is located. The mean equivalent diameter of hydrates is obtained from

$$\beta_V^{\mathrm{H}} = C \frac{\pi d^3}{6} \quad (11)$$

Even though the experiments have been carried out by using a solution with a composition near the composition of the congruent melting point, i.e. $w_{\mathrm{TBAB,\,fus,\,cgr}}^{\mathrm{L_w}} = 1 - w_{\mathrm{w,\,fus,\,cgr}}^{\mathrm{L_w}}$, the modelling calculation take also into account the case of mixture compositions of $0 \le w_{\mathrm{TBAB}}^{\mathrm{L_w}} \le w_{\mathrm{TBAB,\,fus,\,cgr}}^{\mathrm{L_w}} = w_{\mathrm{TBAB,\,max}}^{\mathrm{L_w}}$. Therefore, another concentration quantity is introduced based on the defined reference state of the composition at the congruent melting point. The model considers the liquid phase mass fraction of water in excess of the weight fraction at the congruent melting point, abbreviated as $w_{\mathrm{w,\,free}}^{\mathrm{L_w}}$, the so-called mass fraction of free water. Its value is a linear function of $w_{\mathrm{TBAB}}^{\mathrm{L_w}}$, the mass fraction of TBAB in the residual solution and related to the hydration number ν_{w} according to

$$w_{\mathrm{w,\,free}}^{\mathrm{L_w}} = 1 - w_{\mathrm{TBAB}}^{\mathrm{L_w}} \left(1 + \frac{\nu_{\mathrm{w}} M_{\mathrm{w}}}{M_{\mathrm{TBAB}}} \right) \qquad (12)$$

In the present case, the weight fraction range for possible TBAB compositions covers the range $0 \le w_{\mathrm{TBAB}}^{\mathrm{L_w}} \le w_{\mathrm{TBAB,\,max}}^{\mathrm{L_w}} = w_{\mathrm{TBAB,\,fus,\,cgr}}^{\mathrm{L_w}} = M_{\mathrm{TBAB}} / (M_{\mathrm{TBAB}} + \nu_{\mathrm{w}} M_{\mathrm{w}})$, equivalent to values for $w_{\mathrm{w,\,free}}^{\mathrm{L_w}}$ in the interval $1 = w_{\mathrm{w,\,free,\,max}}^{\mathrm{L_w}} \ge w_{\mathrm{w,\,free}}^{\mathrm{L_w}} \ge 0$.

Since the hydrate crystals are assumed to be in local equilibrium with the surrounding solution, $w_{\mathrm{w,\,free}}^{\mathrm{L_w}}$ is related to the equilibrium temperature. The relation between $w_{\mathrm{w,\,free}}^{\mathrm{L_w}}$ and T is obtained from the equilibrium curve of Fig. 1 and Eq. (12). For a congruent mixture (41 wt% of TBAB), the excess water mass fraction $w_{\mathrm{w,\,free}}^{\mathrm{L_w}}$ is zero during crystallisation. For a lower initial TBAB mass fraction, $w_{\mathrm{w,\,free}}^{\mathrm{L_w}}$ increases with proceeding crystallisation and decreasing temperature. Only hydrates of A type (ν_{w} = 26) are considered in the model. Indeed, the TBAB mass fraction of the solution used in this study has been close to the concentration at the congruent melting point. The model remains valid between 9.6 °C and 12.4 °C and for solutions possessing initial TBAB weight fractions ranging from 20 % to 40 % where theoretically only A type hydrates should be encountered.

The mass of water in excess per unit of volume of the slurry is given by $(1 - \beta_V^{\mathrm{H}}) \rho_{\mathrm{sol}} w_{\mathrm{w,\,free}}^{\mathrm{L_w}}$, and, hence, the following balance equation can be set up for the “free water”

$$\frac{\partial}{\partial t} \left[A_{\mathrm{s,\,tank}} \left(1 - \beta_V^{\mathrm{H}} \right) \rho_{\mathrm{sol}} w_{\mathrm{w,\,free}}^{\mathrm{L_w}} \right] + \frac{\partial}{\partial Z} \left[A_{\mathrm{s,\,tank}} \left(1 - \beta_V^{\mathrm{H}} \right) \rho_{\mathrm{sol}} \left(w_{\mathrm{w,\,free}}^{\mathrm{L_w}} v_{\mathrm{sol}} - D_{\mathrm{eq,\,w,\,free}} \frac{\partial w_{\mathrm{w,\,free}}^{\mathrm{L_w}}}{\partial Z} \right) \right] = 0 \qquad (13)$$

The source and the sink terms occurring in the three conservation equations (Eqs. (9), (10) and (13)) correspond to the inlets and outlets of the tank, respectively, which are calculated from the operating conditions in the hydrate generation and utilisation loop, respectively.

These constitutive equations are discretised by means of a semi-implicit finite volume approach and numerically solved by using Matlab®.

4. Results

4.1. Hydrate generation

During the experiments, the scraped surface heat exchanger is able to produce hydrate slurries attaining a solid phase weight fraction of up to approximately 12 % at the generator outlet. This average value has been determined from calorimetric measurements after sampling. The TBAB solution does only circulate in the closed loop between the storage tank and the hydrate generator. In our experiments, the air-conditioning system had been turned off during the generation of the hydrates. The initial overall weight fraction of TBAB in the solution $w_{\mathrm{TBAB,\,0}}^{\mathrm{L_w}}$ amounts to 0.39 and, hence, is not too far away from the corresponding value at the congruent melting point $w_{\mathrm{TBAB,\,fus,\,cgr}}^{\mathrm{L_w}} = M_{\mathrm{TBAB}} /(M_{\mathrm{TBAB}} + \nu_{\mathrm{w}} M_{\mathrm{w}}) = 0.4007$. Since in the neighbourhood of the congruent melting point, the temperature varies only a little (the H-L_w equilibrium curve is very flat as can be verified in the phase diagram presented in Fig. 1), the dissociation temperature of the TBAB-semi-clathrate hydrate co-existing in H-Lw equilibrium with a solution at $w_{\mathrm{TBAB}}^{\mathrm{L_w}} = 0.39$ is quasi constant and almost identical with the congruent melting temperature $\vartheta_{\mathrm{hyd,\,fus,\,cgr}} = \vartheta_{\mathrm{hyd,\,dis,\,cgr}} = 12.4°\mathrm{C}$. Initially, the temperature in the tank amounts to approximately 19 °C.

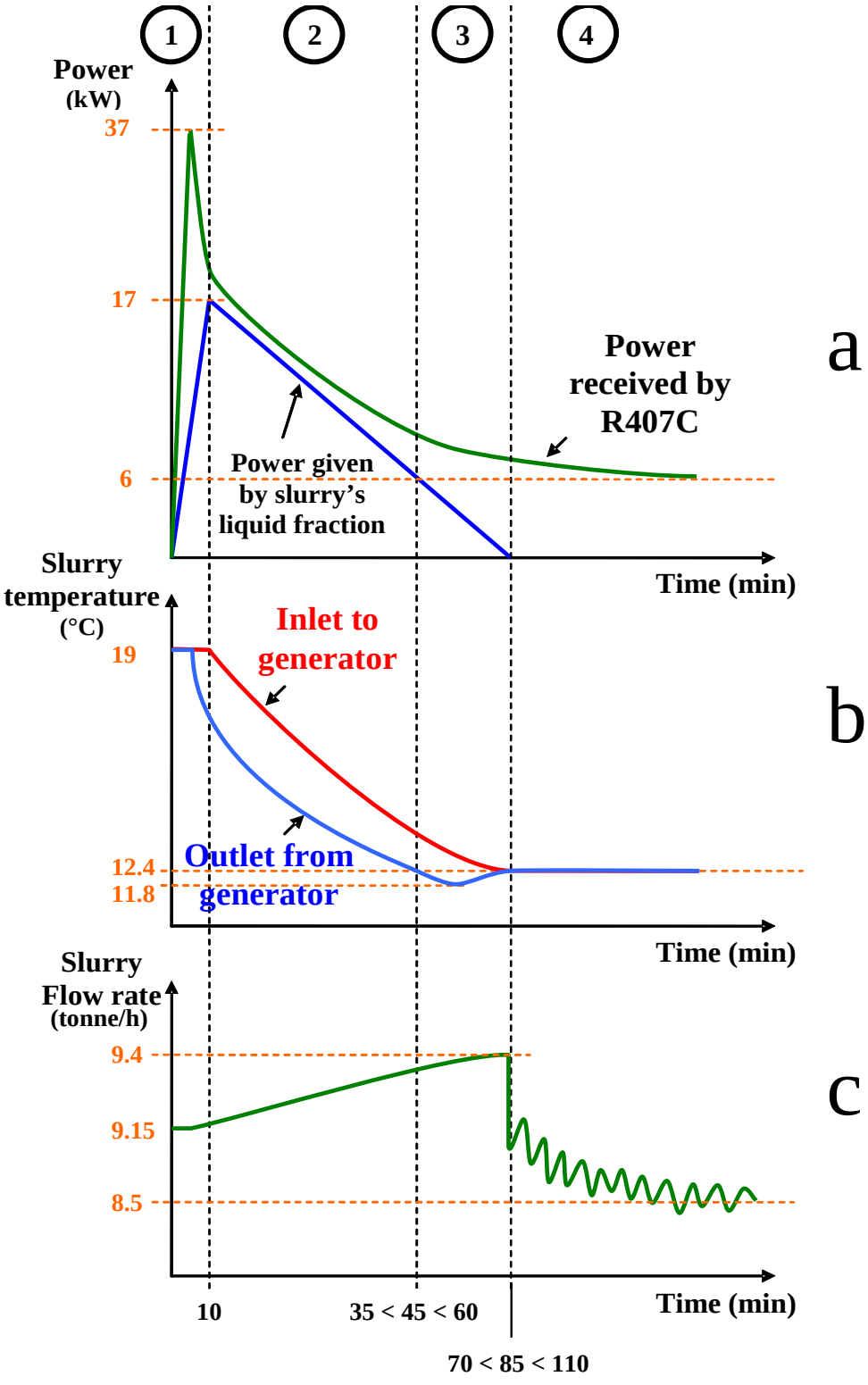

Fig. 6 Schematic representations of thermal powers, temperatures and flow-rate recorded for the cooling media in the generation loop as function of time.

The generation step turned out to be reproducible. Fig. 6 gives the tendencies observed during this step for the thermal powers, the temperature and the mass flow rate of the slurry as function of time. Fig. 6 (a) presents the evolution of the thermal power calculated from the temperature drop of the liquid fraction circulating through the crystalliser. At the initial stages of the generation step, the circulating solution appears to remain completely in the liquid state. Before the crystallisation in the liquid solution starts, it is possible to estimate the cooling power from an analysis of the temperature drops (Fig. 6 (b)) as well as by flow-rate measurements (Fig. 6 (c)). The cooling power of the liquid TBAB solution, $P_{\text{TBAB solution}}$, can be estimated according to the following relation

$$P_{\text{sol}} = \dot{m}_{\text{sol}} \bar{c}_{p,\text{sol}} \left(T_{\text{inlet}} - T_{\text{outlet}} \right) \quad (14)$$

where $\dot{m}_{\text{TBAB solution}}$ denotes the mass flow-rate of the liquid TBAB solution, $\bar{c}_{p,\text{sol}}$ the specific heat capacity of the TBAB solution, and T_{inlet} and T_{outlet} the temperatures measured at the inlet and the outlet of the slurry generator, respectively. For a TBAB solution possessing the composition of the congruent melting point of the corresponding semi-clathrate hydrate (with a hydration number of $\nu_{\text{w}} = 26$) it was shown that the specific heat capacity of the aqueous solution above the equilibrium temperature amounts to about 3.6 kJ kg^{-1} K^{-1}.

Fig. 6 (a) does also present the cooling capacity of the primary refrigerant R407C which is delivered to the crystalliser by evaporation. This power is given by the product of the flow-rate of the primary refrigerant and the change in enthalpy it undergoes upon evaporation

$$P_{\text{R407C vap}} = \dot{m}_{\text{R407C}} \left(h^{\text{L}}_{\text{R407C, inlet}} - h^{\text{V}}_{\text{R407C, outlet}} \right) \quad (15)$$

In Eq. (15), $P_{\text{R407C vap}}$ stands for the cooling capacity of the primary refrigerant R407C, $\dot{m}_{\text{R407C}}$ for its corresponding mass flow-rate, and $h^{\text{L}}_{\text{R407C, inlet}}$ and $h^{\text{V}}_{\text{R407C, outlet}}$, for the specific enthalpy of

R407C in the liquid and in the vapour phase, respectively. The flow-rate has been determined experimentally by means of a mass flow-meter. The enthalpy change of the fluid has been calculated from results of measurements of temperature and pressure at the entry and at the exit of evaporator (inside the generator), respectively. The enthalpy change of the fluid (R407C) is calculated using the "Engineering Equation Solver" (EES provided by F-Chart Software), which also includes a library of thermodynamic properties of several fluids. Fig. 6 (b) presents the slurry temperatures at the inlet and outlet of the generator. The inlet temperature corresponds to the temperature of the slurry coming from the storage tank. The outlet temperature is the temperature of the solution or slurry at the exit of the generator before it is re-injected into the storage tank. The diagram of Fig. 6 (c) displays a plot of the mass flow-rate of the solution or the slurry circulating between the storage tank and the generator as function of time.

In step 1, during the first 10 minutes, the evaporating power (or cooling capacity) of the primary refrigerant increases and achieves its maximum value at around 37 kW. Subsequently, the evaporating power drops rapidly before at some point of time at around 10 min it decreases more slowly – following the same trend as the one being observed for the cooling power of the TBAB aqueous solution.

In step 2, over the time interval ranging from around 10 min up to approximately 45 min, the curve displaying the evaporating power of the conventional cooling fluid R407C and the cooling power curve of the secondary {H_2O + TBAB} based cooling medium follow the same trend (Fig. 6 (a)). During this period, the cooling power of secondary fluid is slightly smaller than the corresponding power related to the evaporation capacity of the primary fluid R407C. This is partially due to heat losses in the crystalliser, but also due to the formation of compact

hydrate layers on the surfaces of cooling plates. These layers have been detected by visual observation though the windows of the hydrate generator. As a consequence of this complication the heat transfer drops. This drop in heat transfer explains the decrease of both the evaporating capacity and cooling power of secondary cooling medium. The inlet temperature (temperature of the fluid exiting the storage tank) decreases due to the removal of heat from the tank cooled via the closed generation loop (Fig. 6 (b)). Since the temperature is higher than 12.4 °C, the circulating mixture remains in the liquid state and the outlet temperature decreases according to Eq (14). In the same period of time, the flow-rate of TBAB solution increases simultaneously as shown in Fig. 6 (c). In fact, the temperature drop of the solution causes a moderate increase of its viscosity. This increase in viscosity leads to an enhancement of the performance of the volumetric pump P3.

In Step 3, after around 45 minutes, the outlet temperature attains the value of 12.4 °C. At this temperature, the temperature of the congruent melting point at atmospheric pressure, TBAB-semi-clathrate hydrate crystals become theoretically stable. Nevertheless, at that stage, the semi-clathrate hydrate phase does not precipitate from the TBAB solution yet. Instead, the temperature of the liquid at the outlet of the crystalliser continues to decrease and hence attains the super cooled state. This phenomenon has also been observed by JFE Engineering Corp. on their systems (Mitzukami, 2010). Then, at approximately 85 min, inlet and outlet temperatures approach the corresponding value of the liquid-solid equilibrium and, hence, the temperature becomes uniform in the crystalliser as well as in the reservoir tank.

At this stage (step 4), after around 85 minutes, semi-clathrate hydrate particles start to form in the {H_2O + TBAB} mixture causing its state to change from a liquid solution to a slurry. The continuous increase in the solid phase fraction of the secondary cooling fluid leads to a rise in

its viscosity (Darbouret, 2005a and Darbouret et al., 2005b) which in turn is responsible for the decrease in flow-rate suddenly observed. On the contrary, the oscillations reported by the flow-meter can to our opinion not be related to true oscillations in flow-rate. Instead, those oscillations are rather believed to reflect a problem inherent to the experimental technique, since the instrument used in these measurements is not designed to accurately monitor the flow of two-phase fluids. After a while, the cooling capacity approaches a limiting value of 6 kW, which is determined by the decrease in heat transfer due to the continuous formation of hydrate layers on the plates of the crystalliser. At around 5 hours, the compact hydrate layers attain such a thickness that they cause the blockage of the scrappers. The experiment is stopped when this blockage is detected to prevent any technical problems (overheating of the motor scrappers, bad circulation in the generation loop, too great decline of the evaporation temperature of the primary fluid and damage of the compressor of the primary loop). At the end of the experiment, the mass-based hydrate phase fraction β_m^{H} amounts to approximately 12 %.

The formation of the compact hydrate layers is probably caused by the great difference between the temperature of the refrigerant (≈ –30 °C at the end of the experiments) and the temperature of the slurry (12.4 °C). Technical modifications which aim at reducing this difference by an appropriate regulation of the cooling capacity of the primary loop are currently under development.

No complications were observed with regard to the flowing of the TBAB hydrate slurry within the generation loop. This observation confirms previous results obtained at the laboratory scale (Darbouret, 2005a and Darbouret et al., 2005b). The volumetric pump P3 works well and handles the slurry without any difficulties.

4.2. Utilisation loop

After crystallisation and storage, the hydrate slurry is delivered to end-users. In these secondary cooling cycles, the semi-clathrate hydrate particles are progressively molten, which typically, like in the pilot plant used here, takes places in fan coils. The results of first measurements are presented in Fig. 7. In this experiment, three of four rooms, corresponding to a total surface area of 100 m^2, were air-conditioned. In the plots of the corresponding diagram, the temperature of the cooling slurry is displayed as function of time, as measured by three selected temperature sensors (T1, T4, and T6). These three sensors are located at different sites in the distribution loop (see Fig. 4), which possesses a total length of 100 m. T1, T4 and T6, are located at the tank exit, the middle of the distribution loop and the tank inlet, respectively.

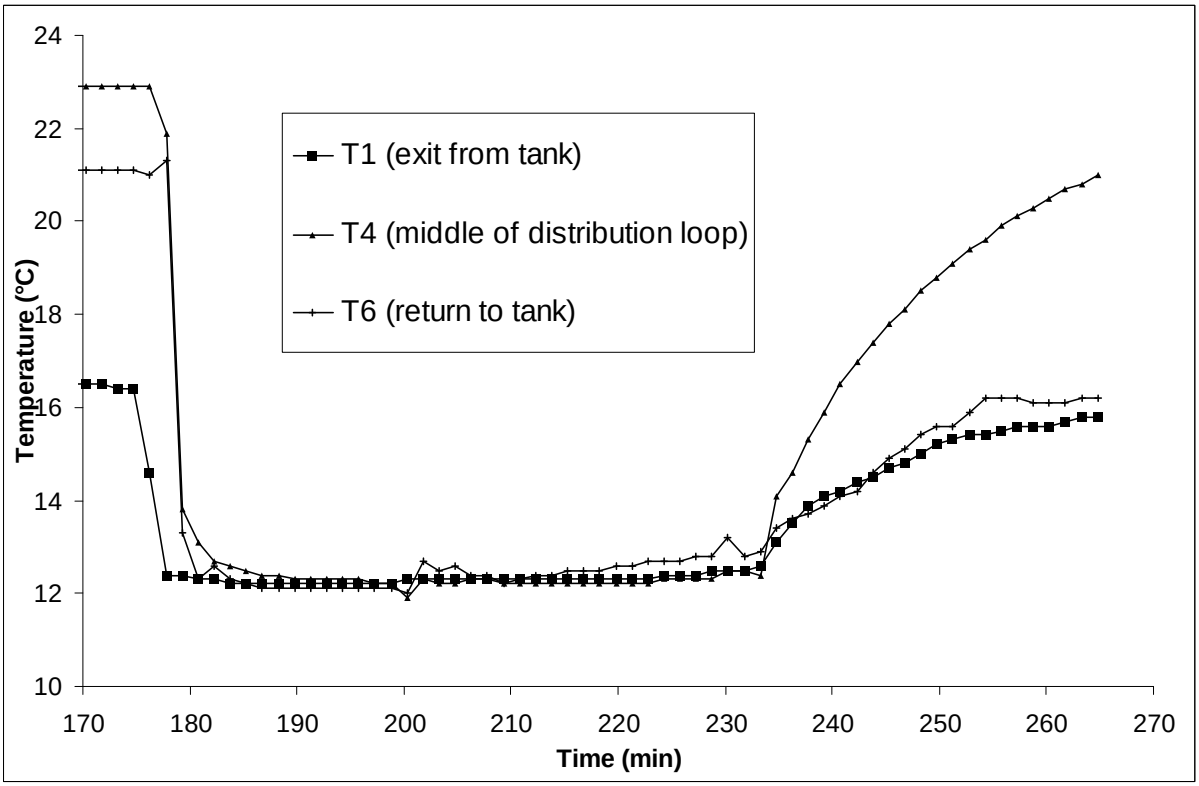

Fig. 7 Recordings of temperatures measured at different locations in the distribution flow loop (at temperature sensors T1, T4 and T6 at the tank exit, the middle of the distribution loop and the tank inlet, respectively) during the utilisation period.

The initial hydrate phase fraction of the slurry in the storage tank is determined to 12 wt% (at 180 min in Fig. 7). This value has been measured on samples taken from the content of the storage tank by means of calorimetric measurements. In our experiments, the distribution loop has been run for cooling three rooms. The temperature of the circulating slurry possesses the value of 12.4 °C, which corresponds to the temperature at the normal congruent melting point. The temperatures determined at three different measuring points (located at the tank exit, the middle of the distribution loop and the tank inlet, respectively) remain constant for approximately 1 h. After, (around 235 min in Fig. 7), the temperatures at these measuring locations exhibit a sudden increase, which it is due to the fact that at this point the hydrate in the storage tank has completely molten.

4.3. Hydrate storage in the tank

The slurry was maintained in its original state during the daily storage. No problem have been encountered with regard to the storage of the hydrate slurry, e. g., the hydrate particles did not agglomerate to form a plug.

However, during wintertime, the temperatures usually decrease to reach values of below 12.4 °C and, hence, under these conditions, crystallisation does occur naturally in our machine room. When, upon arrival of the warmer seasons, the average ambient temperature increased above 12.4 °C, no damages had been observed in the tank, however, the pipes were

slightly damaged. In fact, the density of the TBAB-semi-clathrate hydrate structure is higher than the density of the corresponding liquid solution. Hence, upon melting of the massive amounts of solid semi-clathrate hydrate that have been accumulated in the system during crystallisation, the overall volume of the {H_2O + TBAB} mixture increases which can lead to a swelling of the pipes. In the pipes of our plant local deformations of this kind, i.e. deformations being caused by this phenomenon have been observed.

4.4. Modelling results and comparison with measurements

4.4.1. Model parameters

A schematic representation of the design of the storage tank emphasising its geometrical configuration, is given in Fig. 8.

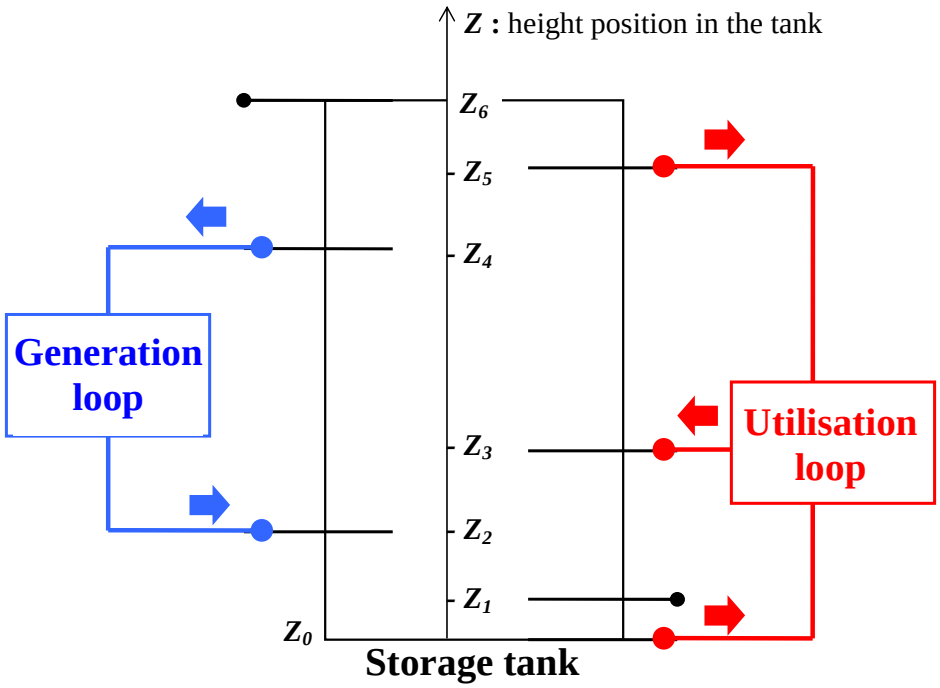

Fig. 8 Locations of “inlet loops” and “outlet loops” on the storage tank.

The numerical values for the physical parameters used in the model calculations are summarised in Table 2. The technical parameters (flow-rates and cooling capacities) were obtained experimentally.

Table 2 Model main input parameters.

Parameters	Numerical values
Initial mass fraction of TBAB	0.39
Volumetric flow-rate in generation loop	10 m^3 h^{-1}
Total volumetric flow-rate in distribution loop	4 m^3 h^{-1}
Viscosity of aqueous solution (at the congruent melting point)	1.3×10^{-2} Pa s
Equivalent diffusivities	10^{-7} m^2 s^{-1}
Specific latent heat of fusion of the semi-clathrate hydrate	193 kJ kg^{-1}
Generated hydrates diameter	100 μm
External temperature	20 °C
Global heat transfer coefficient (trough lateral insulation)	1.84 W m^{-2} K^{-1}
Generated cooling capacity (generation loop)	300 000 $t^{-1/2}$ (in W for *t* in s)
Consumed cooling capacity (utilisation loop)	10 kW

The operation mode of the plant is to be described as follows:

- A first period of 180 minutes during which only the generation loop is operating ("generation period")

- A second period of 120 minutes which concerns the distribution loop only. In this step, the rooms to be air-conditioned are cooled by using the second cycle based on the hydrate slurry as cooling medium ("utilisation or distribution period")

4.4.2. Modelling results

In the first graph of Fig. 9, the total (cumulative) cooling capacity (or total stock in kWh) corresponding to the enthalpy change upon hydrate dissociation of the total amount of Phase Change Material accumulated in the storage tank is plotted against time. During the first 3 hours the amount of semi-clathrate hydrate in the tank increases at a slowly diminishing rate. This is time interval of semi-clathrate hydrate production which is referred to as the "generation period". The subsequent decrease in rate is caused by the decrease in the cooling capacity, also called "generation power" as in the second graph of Fig. 9, which in turn is the result of the drop in heat transfer. As outlined previously, compact hydrate layers form on the surfaces of the generator plates, and thereby continuously cause a decrease in the efficiency of heat transfer (see the generated cooling capacity in Table 2).

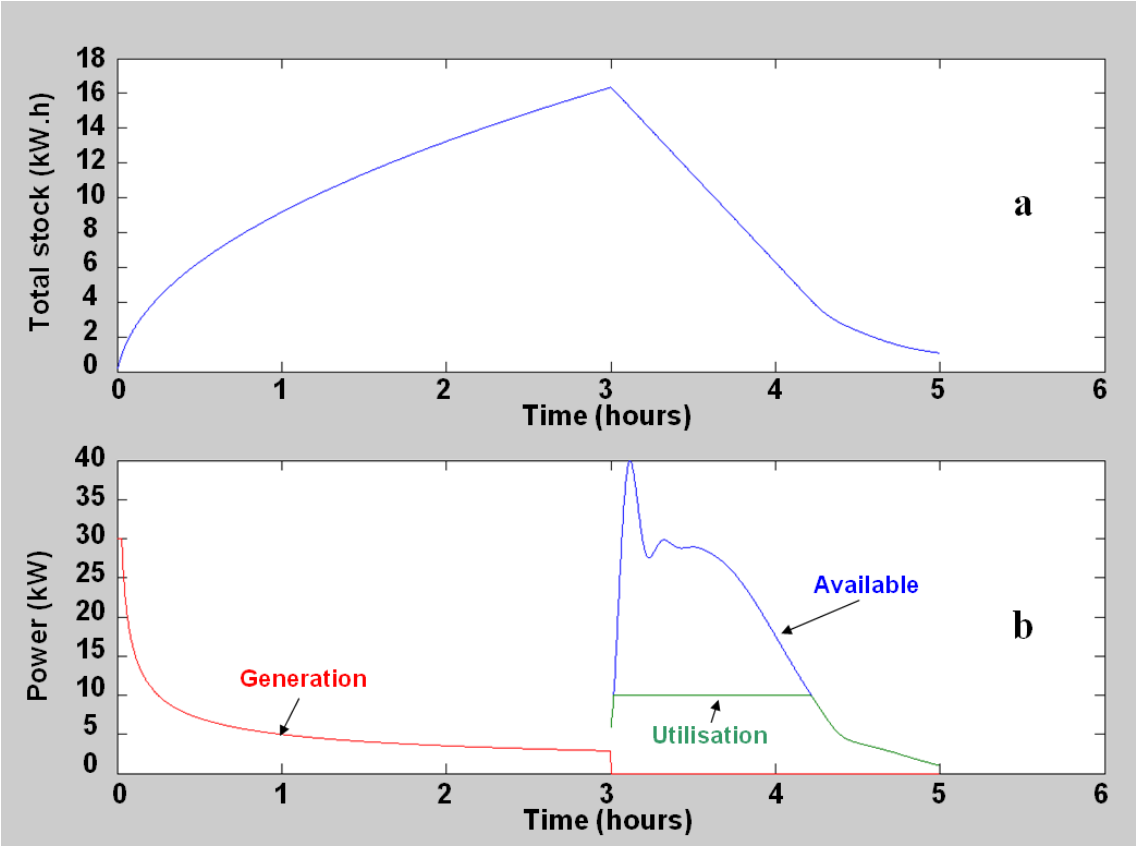

Fig. 9 General results of the model calculations.

After 3 hours, the production of semi-clathrate hydrate is stopped, and the utilisation loop is started to distribute the slurry to the end-user. It is assumed that the cooling duty is 10 kW which corresponds to a total area of around 100 m^2 (in accordance with the experiments, three of the four rooms have been considered in the air-conditioning model calculations). The cooling capacity of the slurry in the utilisation loop, referred to as the "available power" in the second graph of Fig. 9, is proportional to the mass-based phase fraction of semi-clathrate hydrate and flow-rates in the loop. Whereas the flow-rates are constant, the solid phase fraction in the two suction zones of the storage tank varies with time. During the first 10 minutes of the utilisation period, the available power oscillates before it stabilises. Subsequently it begins to decrease in relation to the global decrease of the total stock available. However, the available power in Fig. 9, still remains higher than the need of 10 kW during more than one hour. This means that after a complete cycle of a given portion of the slurry in the utilisation loop, the hydrate crystals contained in this element are not completely melted. In other words, after having undergone a full cycle, a certain fraction of the semi-clathtrate hydrate particles are recycled to the storage tank.

As long as the hydrate content is sufficiently high to supply 10 kW of cooling capacity, the total stock of PCM in the tank decreases linearly. The heat losses of the storage tank are negligible. After 80 min of distribution, the available power falls below the need of 10 kW because the phase fractions of solid in the suction zones are not high enough. In the utilisation loop, all the slurry is molten and only a liquid solution flows back again into the storage tank. Fig. 10 and Fig. 11, respectively, give more details on the local characteristics of the slurry in the storage tank during semi-clathrate hydrate generation (Fig. 10) and utilisation (Fig. 11). The vertical axe represents the height up to which the storage tank is filled.

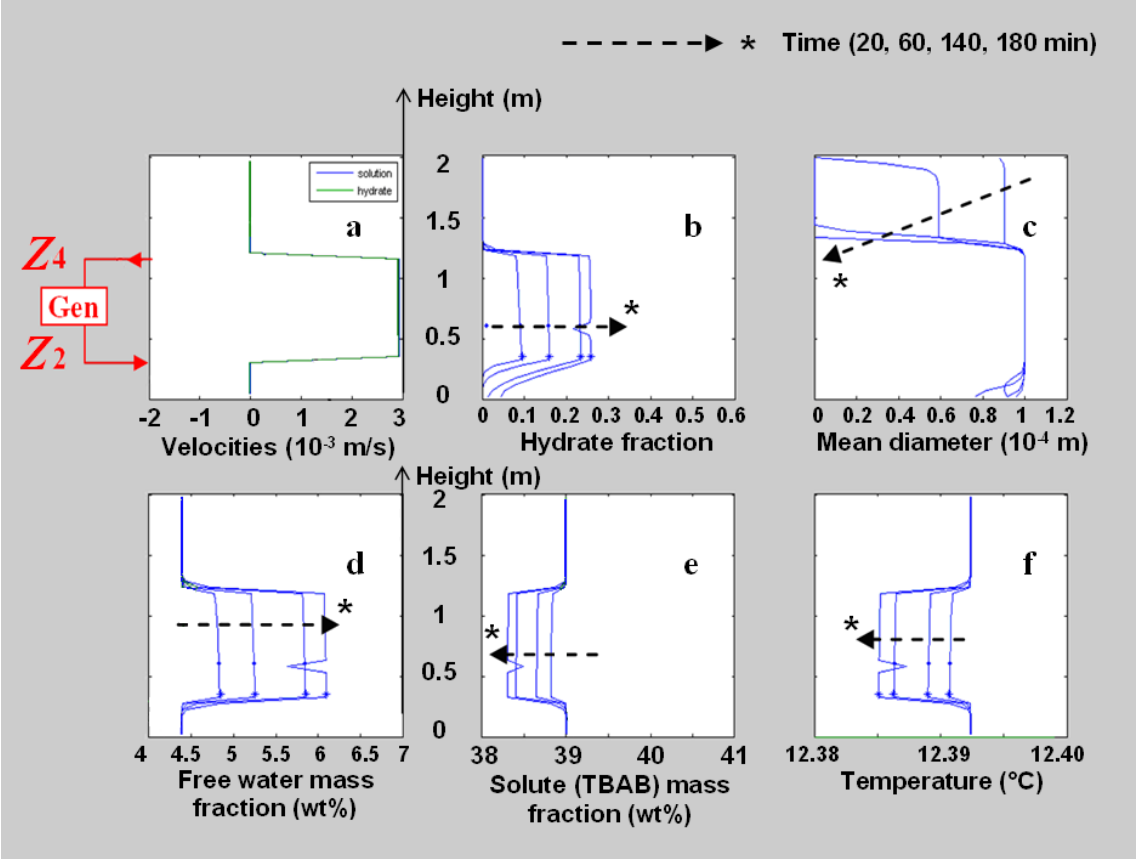

Fig. 10 Modelling results during the generation period.

In the diagrams of Fig. 10, four curves are plotted in each graph corresponding to four different points of time in the time interval covering the hydrate generation. The curves have been calculated at (20, 60, 140 and 180) min. The velocity of the liquid solution and the semi-clathrate hydrate particles, respectively, is displayed diagram (a) of Fig. 10. Since the settling velocity is very low, these two curves appear to be identical. There is a vertical flow which corresponds to the flow induced by the outlet located at height Z_4 = 1.2 m towards the hydrate generator, and by the inlet at height Z_2 = 0.4 m where the slurry is flowing back from the generator). In diagram (b) the height is plotted against the hydrate phase fraction. In this graph it can be observed that the solid is principally accumulated in the space determined by the cross sections between the outlet and the inlet. But, due to the settling of the hydrate particles, even if low, a certain fraction of the solid succeeds in accumulating at the bottom, below Z_2.

In between the heights Z_4 and Z_2, the particles have a diameter corresponding to the size attained immediately after their formation in the generation step (100 μm, see Table 2). In this zone, heat losses through the wall are not sufficiently high for melting the crystals and decrease their size significantly. At the bottom as well as in zones which are not submitted to the heat convection from the hydrate generator, particles are present in lower concentration. Due to the partial melting of the semi-clathrate crystals their mean diameter also decreases to some extent. The top of the tank is not affected by the settling but only by the diffusion of particles. As a consequence of this, only few crystals are encountered in this region. The average diameter of these crystals assumes a relatively small value due to the fact that the particles found at these heights do melt more easily.

The free water mass fraction, or equivalently, the mass fraction of the solute (TBAB), and the temperature are mutually linked by the equilibrium curve (Fig. 1). As long as the system is biphasic, exhibiting a liquid aqueous solution L_w and a solid semi-clathrate hydrate phase S ≡ H in combined phase and dissociation equilibrium, the temperatures and concentrations lie on the equilibrium curve. Since the crystallisation is started close to the point of the congruent semi-clathrate hydrate dissociation, the temperature variations are very small, amounting to values of less than 0.01 °C (see Fig. 10 (f)). Hence, the respective free water as well as the solute mass fraction in the liquid solution vary also very little as can be seen in diagrams (d) and (e) of Fig. 10. These variations in concentration do only concern the zone located in between Z_4 and Z_2.

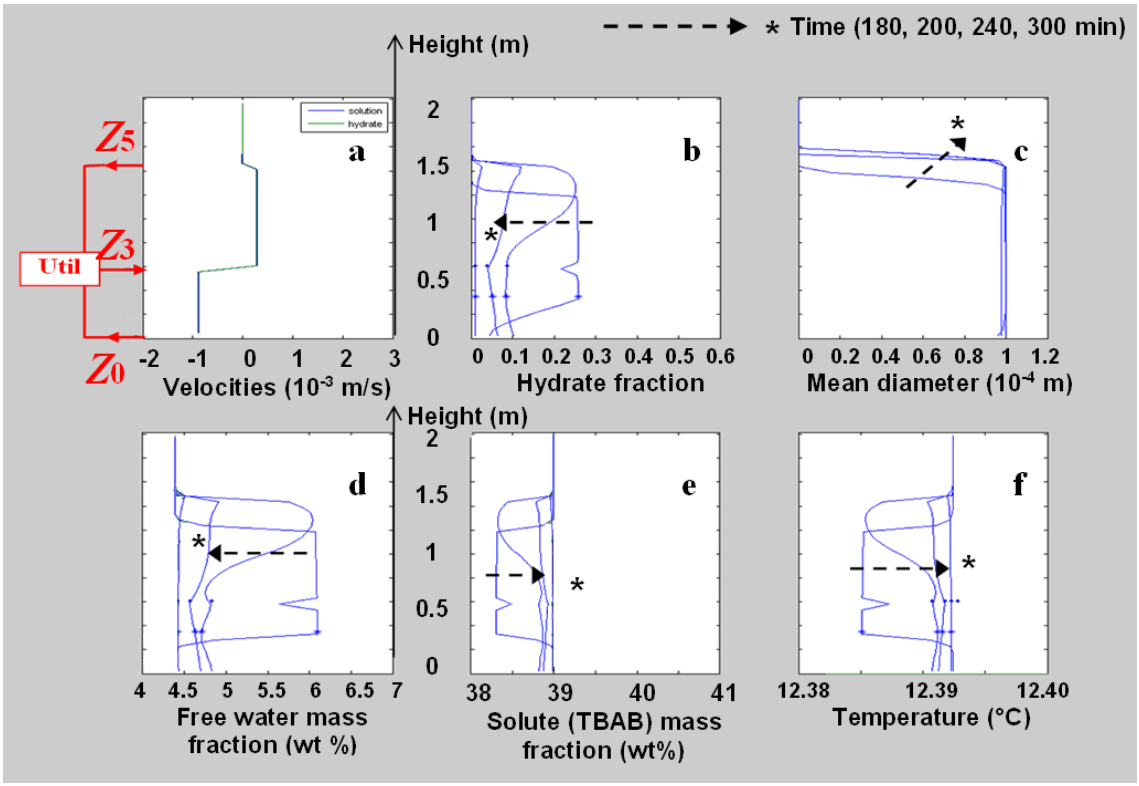

Fig. 11 Modelling results during utilisation period.

In Fig. 11, the same curves as shown in Fig. 10 are presented for the subsequent time interval of the utilisation period ranging from 180 min to 300 min. In each of the diagrams of Fig. 11, the height Z is plotted against the velocities of the liquid solution and the semi-clathrate hydrate particles (diagram (a)), the hydrate phase fraction (diagram (b)), the mean diameter (diagram (c)), the liquid phase free water mass fraction and solute TBAB mass fraction (diagrams (d) and (e)) and the Celsius temperature (diagram (f)), respectively. The four curves displayed in each of the graphs (b)-(f) of Fig. 11, respectively, correspond to the profiles calculated at t = 180 min, 200 min, 240 min and 300 min. The suction heights are located at the bottom and the top of the reactor, located at Z_0 = 0 and Z_5 = 1.4 m, respectively. At Z_3 = 0.6 m the slurry flows back. At the level of Z_0, the outlet flow-rate is 3 m^3 h^{-1} whereas at Z_5 it is 1 m^3 h^{-1}. Hence, the flow-rate of the quasi-incompressible slurry detected at the inlet at Z_3 where it enters the tank again amounts to 4 m^3 h^{-1}. The velocities in the storage tank

calculated for heights between Z_3 and Z_5 are positive. In other words, the resulting flow of the slurry is oriented in upwards direction. In the region between Z_3 and Z_0 the current velocity of the fluid flow is directed downwards. In terms of its absolute value, the mean velocity in the upward flow found between Z_3 and Z_5 amounts to one third of the absolute value of mean velocity characterising the downward flow encountered between Z_3 and Z_0. As a consequence of this, the bottom zone (below Z_3) is exhausted more rapidly than the top zone (above Z_3): the hydrate phase fraction remains greater in the top zone than in the bottom zone. The minimum in the hydrate phase fraction will be found at the level of the inlet at Z_3 since a partially or completely molten slurry is re-introduced at this level. The mode of operation during the utilisation period, i.e. the stationary circulation of the hydrate suspension results in a spatial homogenisation of the slurry. On the microscopic level this observation corresponds with the uniform distribution (see Fig. 11 (c)) of the mean hydrate crystal diameter along the complete height of the tank (Z_0 and Z_5).

The curve plotted for t = 180 min is common to both Fig. 10 and Fig. 11. It corresponds to the point of time at which the utilisation loop has been started. The shape of the curve reflects the sudden and relatively great local variation of the mass-based hydrate phase fraction around Z_3, the height of the inlet. Through that inlet the slurry, is recycled. Since the recycled slurry is partially melted, its liquid phase fraction is enriched in TBAB. Consequently, the liquid phase being present in the zone around Z_3 is more concentrated in TBAB in comparison to the rest of the tank.

4.4.3. Comparison between measured and modelling results

At the end of the generation period, as can be seen Fig. 9 (a), the total amount of cooling capacity has achieved a value close to 16 kWh. The corresponding slurry in the tank possesses a hydrate phase fraction of approximately 16 wt%. The numerical value for the mass-based hydrate phase fraction predicted by the model which amounts to 16 % exceeds the corresponding experimental result of ≈ 12 %. This is probably mainly due to imperfections inherent in the modelling approach since the latter does not take into account the first step of cooling the liquid from ambient temperature at around 19 °C to the crystallisation temperature of 12.4 °C. In fact, the model considers that the solution is already in the state corresponding to the liquidus curve at the beginning of the generation period. As a consequence of the overestimation of the stored energy the model predicts a longer duration for the air-conditioning period (80 min compared to 60 min observed in section 4.2).

Despite these differences between experimental and predicted results, the model is able to predict the main tendencies with regard to the cooling characteristics of our plant. The model enables the execution of parametric studies. First comparisons with the results obtained from experimental studies carried out on our prototype are encouraging. The model confirms that the positions of the outlet and inlet of each loop are important for the final design of the tank. The prototype needs to be regulated at the level of the primary loop in order to prevent the formation of a compact hydrate layer on the surfaces of the heat exchanger plates of the hydrate generator.

5. Conclusion and Outlook

This work confirms the feasibility of an air-conditioning system using a slurry of TBAB-based semi-clathrate hydrate as secondary refrigerant. We adapted a technology designed for

the generation of ice slurries. Some technical problems will still have to be solved; however, different solutions are currently being tested. The main difficulty lies in finding ways to prevent the formation of a compact semi-clathrate hydrate layer on the plates of the heat exchangers in the generation unit.

A model has been developed in order to predict the amount of hydrate and its distribution in the tank. The comparison between numerical and experimental results is encouraging. It enables to propose new designs, especially with regard to the positions of the inlet and outlet pipes.

After modifications, the model parameters will be refined. The model will be used to simulate new alternative configurations, as for example initial TBAB solutions at other concentrations. For the best predicted configuration, series of measurements will be carried out in order to test the performance of the model calculations experimentally.

Acknowledgements

This study has benefited from the financial support of the “Cluster Energie” - Région Rhône Alpes (France). Technical support has been supplied by Lennox-Europe and HeatCraft-Europe.

In memory of Gérard Blain, technician at Heatcraft Compagny, who has made a significant contribution to this work.

References

Belandria, V., Mohammadi, A. H., Richon, D., 2009. Volumetric properties of the (tetrahydrofuran + water) and (tetra-n-butyl ammonium bromide + water) systems: Experirental measurements and correlations. J. Chem. Thermodyn. 41, 1382-1386.

Ben Lakhdar, M. A., Melinder, Å., 2002. Facing the challenge to produce ice slurry for freezer applications. 5th IIR Workshop on Ice Slurries, Stockholm, Sweden.

Ben Lakhdar, M. A., Cerecero, R., Alvarez, G., Guilpart, J., Flick, D., Lallemand, A., 2005. Heat transfer with freezing in a scraped surface heat exchanger. Appl. Therm. Eng. 25, 45-60.

Compingt, A., Blanc, P., Quidort, A., 2009. Slurry for Refrigeration Industrial Kitchen Application. Proceedings of 8th IIR Conference on Phase Change Material and Slurries for Refrigeration and Air-conditioning, Karlsruhe, Germany.

Darbouret, M., 2005a. Etude rhéologique d'une suspension d'hydrates en tant que fluide frigoporteur diphasique Résultats expérimentaux et modélisation. Thèse de doctorat, Génie des Procédés, Ecole Nationale Supérieure des Mines de Saint-Etienne, France.

Darbouret, M., Cournil, M., Herri, J. M., 2005b. Rheological study of TBAB hydrate slurries as secondary two-phase refrigerants. Int. J. Refrig. 28 (5), 663-671.

Dumas, J. P., 2002. Stockage du froid par chaleur latente. Techniques de l'Ingénieur, BE9775.

Dyadin, Y. A.; Udachin, K. A., 1984. Chlathrate formation in water-peralkylonium salts systems. J. Inclusion Phenomena 2, 61-72

Gibert, V., 2006. Ice Slurry, Axima Refrigeration Experience. 7th Conference on Phase Change Materials and Slurries for Refrigeration and Air-conditioning, 13-15, Dinan, France.

Kumano, H., Hirata, T., Kudoh, T., 2011a. Experimental study on the flow and heat transfer characteristics of a tetra-n-butyl ammonium bromide hydrate slurry (first report: Flow characteristics). Int. J. Refrig. 34, 1963-1971.

Kumano, H., Hirata, T., Kudoh, T., 2011b. Experimental study on the flow and heat transfer characteristics of a tetra-n-butyl ammonium bromide hydrate slurry (second report: Heat transfer characteristics). Int. J. Refrig. 34, 1963-1971.

Lipkowski, J., Komarov, V. Y., Rodionova, T. V., Dyadin, Y. A., Aladko, L. S., 2002. The structure of TetraButylAmmonium Bromide hydrate $(C_4H_9)_4NBr•21/3H_2O$. J. Supramol. Chem. 2, 435-439.

Meunier, F., Rivet, P., Terrier, M.-F., 2007. Froid Industriel. Dunod, Paris. ISBN 978-2-10-051404-5.

Ma, Z. W., Zhang, P., Wang, R. Z., Furui, S., Xi, G. N., 2010. Forced flow and convective melting heat transfer of clathrate hydrate slurry in tubes. Int. J. Refrig. 53, 3745-3757.

Ma, Z. W., Zhang, P., 2011. Pressure drop and heat transfer characterisics of clathrate hydrate slurry in a plate heat exchanger. Int. J. Refrig. 34, 796-806.

Ma, Z. W., Zhang, P., 2012. Pressure drops and loss coefficients of a phase change material slurry in pipe fittings. Int. J. Refrig. 35, 992-1002.

Mizukami, T., 2010. Thermal Energy Storage system with clathrate hydrate slurry. Keio University “Global COE Program”. International Sympsium, Clathrate Hydrates and Technology Innovations. Challenges Toward a Symbiotic Energy Paradigm, Yokohama, Japan.

Obata, Y., Masuda, N., Joo, K., Katoh, A., 2003. Advanced Technologies Towards the New Era of Energy Industries. NKK Tech. Rev. 88, 103-115.

Ogoshi, H., Matsuyama, E., Miyamoto, H., Mizukami, T., 2010. Clathrate Hydrate Slurry, CHS Thermal energy storage System and Its Applications. Proceedings of 2010 International Symposium on Next-generation Air-conditioning and Refrigeration Technology, Tokyo, Japan.

Oyama, H., Shimada, W., Ebinuma, T., Kamata, Y., 2005. Phase diagram, latent heat, and specific heat of TBAB semiclathrate hydrate crystals. Fluid phase Equilib. 234, 131-135.

Shimada, W., Shiro, M., Kondo, H., Takeya, S., Oyama, H., Ebinuma, T., Narita, H., 2005. Tetra-n-butylammonium bromide-water (1/38). Acta Crystallogr., Sect. C. 61, 65-66.

Takao, S., Ogoshi, H., Matsumoto, S., NKK Corporation, Tokyo (JP), 2001. Air-conditioning and thermal storage systems using clathrate hydrate slurry. US patent - US 6,560,971 B2.

Takao, S., Ogoshi, H., Fukushima, S., Matsumoto, S., JFE Engineering Corp., Tokyo (JP), 2004. Thermal storage medium using a hydrate and apparatus thereof, and method for producing the thermal storage medium. US patent - 20050016200.

Wenji, S., Rui, X., Chong, H., Shihui, H., Kaijun, D., Ziping, F., 2009. Experimental investigation on TBAB clathrate hydrate slurry flows in a horizontal tube: Forced convective heat transfer behaviors. Int. J. Refrig. 32, 1801-1807.

Zhang, P., Ma, Z. W., Wang, R. Z., 2009. An overview of phase change material slurries: MPCS and CHS. Renewable Sustainable Energy Rev. 14 (2), 598-614.